Journal of New Materials for Electrochemical Systems 12, 187-193 (2009)

Effect of Sintering Temperature on the Mechanical Properties of Film $Gd_{0.2}Ce_{0.8}O_{1.9}$ Electrolyte for SOFCs Using Nanoindentation

M. Morales[*,1,2], J. J. Roa[1], X. G. Capdevila[1], M. Segarra[1] and S. Pinol[2]

[1]Departament de Ciència dels Materials i Enginyeria Metal·lúrgica, Facultat Química, Universitat de Barcelona,
\ C/ Martí i Franquès, 1; E-08028, Barcelona, Spain.
[2]Institut de Ciència de Materials de Barcelona (CSIC), Campus de la UAB,
Bellaterra E-08193, Barcelona, Spain.

Received: April 2, 2009, Accepted: August 29, 2009

Abstract: *The mechanical properties of thin film gadolinia doped ceria ($Gd_{0.2}Ce_{0.8}O_{1.9}$, GDC) electrolyte, for solid oxide fuel cells (SOFCs), with different levels of sintering density were investigated by the nanoindentation technique. Electrolyte thin film supported on Ni-GDC cermet was made by co-sintering at several temperatures between 1350 and 1450 ºC. The microstructures of the electrolyte films and the cells performances were studied by scanning electron microscope (SEM) and current-voltage tests, respectively. In order to determine the mechanical properties, a Berkovich indenter was used at different applied loads (30, 50 and 100 mN). Plastic deformation took place, so Oliver and Pharr equations must be applied to evaluate the hardness and Young's modulus of the electrolyte film. The residual nanoindentations were observed by optical microscope (M.O.) and field emission scanning electron microscope (FE-SEM). The present study reveals that the nanoindentation is a non-destructive and ideal technique to determinate the quality and the mechanical properties of the thin film of a SOFC. The results also show that the hardness decreases with the increasing of the applied load, which is attributed to the indentation size effect.*

Keywords: Solid Oxide Fuel Cells (SOFCs), Gadolinia doped ceria (GDC), Electrolyte film, Nanoindentation, Hardness, Young's modulus

1. INTRODUCTION

A solid oxide fuel cell (SOFC) is a device that electrochemically converts the chemical energy of fuels to electricity. SOFCs generally work at 800-1000 ºC in order to obtain high conversion efficiency and power density. Yttria-stabilised zirconia (YSZ) ceramics is the traditional electrolyte material that must typically be operated at high temperatures, due to its relatively high ionic resistivity of the electrolyte at lower ones. However, lowering temperature has a number of potential benefits such as cheaper materials as well as lower degradation problems due to chemical reactivity or thermal shocks. Solid oxide electrolytes based on ceria doped materials are considered one of the most promising candidate materials to be used at low temperature (< 600 ºC), because they have a higher oxygen ion conductivity than YSZ between 500 and 700 ºC [1-4]. Among the doped-ceria materials, GDC ($Gd_{0.2}Ce_{0.8}O_{1.9}$) is one of the most often used electrolytes for SOFCs operating at this temperature range [5]. A second strategy to increase the power density of the SOFCs at low temperature is to decrease the thickness of electrolyte. So, anode-supported thin-film electrolyte fuel cells is a good solution as reported elsewhere [5-9]. For application as a SOFC electrolyte, it is desirable that the sintered electrolyte film has a density greater than 95% of the theorical in order to elude open porosity and avoid reactants cross-over from anode to cathode and vice-versa. In recent years, there has been an increasing interest in examining the sinterability of doped-ceria materials as well as determining its relevant properties for its used as a SOFC electrolyte. Sintering density depends on sintering temperature and time as well as the presence of small amounts of additives and the powders characteristics [10-12]. Many papers have been devoted to the study of the electrical properties of the doped-ceria materials [13-15]. However, few studies have reported the mechanical properties of these materials even using conventional techniques such as Vickers indentation [16-18]. For this reason, this paper is focused on the investigation of the mechanical proper-

*To whom correspondence should be addressed: Email: mmorales@ub.edu

ties of several thin film GDC electrolytes with different levels of sintering density using nanoindentation.

The deformation of a material occurs via two different processes: *i) elastic (reversible) and ii) plastic (permanent) deformation.* Since elastic deformation is a reversible process and related to angstrom scale, it exhibits virtually no dependence on defect size unless a large population of preexisting defects is involved [19]. The plastic deformation occurs as a result of the generation, annihilation, and motion of defects such as dislocations and presents marked size effects when material dimensions are in the range of microns or below.

Nanoindentation is a non-destructive, selective and versatile technique for measuring the mechanical properties at very small scale. At high scale, indentation or hardness testing has long been used for characterization and quality control of materials, but the results are not absolute and depend on the test method. In general, traditional hardness test consists of the application of a single static force with a specified tip shape and material, resulting in a residual impression that has dimensions on the order of few nanometers or micrometers, depending on the applied load. The output of this hardness tester is typically a single hardness value that is a measure of the contact penetration depth of the indentation tip into the sample. Instrumented indentation testing (IIT), also known as continuous-recording indentation or nanoindentation, which means that load and total depth of penetration are measured as function of time during loading and unloading, is a relatively new form to obtain the mechanical properties of a material at nanometric scale. Nowadays, IIT employs high-resolution instrumentation to control continuously and monitor the loads and displacements of an indenter. The method was introduced in 1992 for measuring hardness and elastic or Young's modulus and has been widely used in the characterization of mechanical behaviour of materials at nanometric scales [20-23].

The principal advantage of this technique is that the mechanical properties can be determined directly from indentation load and displacement curves without the need to image the residual impression. Depending on the details of the specific testing systems, loads as small as 1 nN can be applied, and displacements of 0.1 nm can be measured. The most frequently mechanical properties such as hardness, Young's modulus, toughness, yield strength, shear stress and others, can be obtained from the load-displacement curves [20,21,24].

2. EXPERIMENTAL

2.1. Fuel Cell Fabrication

According to our previous studies [25] the electrolyte and anode components of the fuel cell of the present work were composed of GDC with 20 % of Gd_2O_3 and of Ni + GDC (NiO:GDC = 60:40 wt. %), respectively. The cathode was composed of $La_{0.5}Sr_{0.5}CoO_3$ (LSC) + GDC (90:10 wt. %). Anode and LSC powders were prepared by the acrylamide combustion related method, starting from nitrate solutions of the different cations [26,27]. The powders for the $Gd_{0.2}Ce_{0.8}O_{1.9}$ electrolytes were prepared by the sol-gel acetylacetonate reaction technique, starting from acetates as described elsewhere [28]. Finally, 2% in weight of $Co(C_2H_3O_2)_3$ was added in order to reduce the densification temperature of the electrolyte deposited on the anode as described in a previous work [29].

Anode-supported SOFCs were fabricated using a conventional dry pressing technology and dip-coating. The anode powder was compacted under uniaxial pressing to form a disk with a diameter of 11 mm and a thickness of 0.7 mm. Then GDC electrolyte layer was deposited by dip coating on the anode. Subsequently, the bilayers were sintered for 5 h under air atmosphere at various temperatures: 1350 ºC (sample A), 1400 ºC (sample B) and 1450 ºC (sample C). After sintering, all of them were annealed at 900 ºC for 5 h under hydrogen (5%) and argon atmosphere in order to reduce the NiO in the anode to Ni. After the cathode was deposited by dip-coating, the entire structures were sintered at 1000 ºC for 5 h under argon atmosphere. The disk shaped fuel cells had a final diameter of ~10 mm, anode thickness of ~500 μm, electrolyte thickness of ~20 μm and cathode thickness and effective area of ~30 μm and 0.20 cm2, respectively. The cells and electrolyte films were observed with Leica scanning electron microscope (SCT Barcelona).

2.2. Electrical Characterization

Cells performance was evaluated using an in-house built test station. Anode-supported cells were tested in single-chamber configuration (SC-SOFC) placing the cells inside a quartz tube reactor of 22 mm of internal diameter. A Pt wire and a Pt mesh were used as the output terminal and the electrical collector for the anode, respectively, and a Pt wire and a Ag mesh were similarly used for the cathode. Platinum wires were connected to each mesh, serving as voltage and current probes. The cells were operated in single-chamber conditions under optimized gas compositions and flow conditions. A mixture of propane and air with a volume ratio of 1:11 was supplied to the cell at a flow rate of 480 ml min^{-1} between 450 and 650 °C. In addition to the thermocouple that controls the furnace temperature, a second thermocouple attached closely to the anode of the sample was used to determine the cell temperature. Polarization curves were recorded using a Keitley 617 electrometer with an input resistance of 1014 Ω. Currents were determined by measuring the voltage drop in an auxiliary known resistance. Current-voltage tests were carried out by configuring the equipment for measuring current and voltage under variable loads.

2.3. Mechanical Properties

Nanoindentation tests were performed on the polished cross-section of the electrolytes of the cells using a Nano Indenter ® XP System (MTS Systems Corporation) equipped with Test Works 4 Professional level software. The nanoindentations were made by a three-sided pyramid Berkovich diamond indenter. The displacement or penetration depth was continuously monitored and load-time history of indentation recorded. The tip was calibrated with a fused silica standard; the frame stiffness and the thermal drift were automatically corrected. The experiments were carried out at different applied loads: 30, 50 and 100 mN. The loading/unloading time and the peak hold time were selected to be constant for all indentations, 15 and 30 s, respectively. The number of times to load/unload for the different nanoindentation was 5 and the percent to unload was 90%. Each hardness and Young's modulus value is an average of 80 measurements performed on three different samples in order to achieve statistical significance.

The analysis of force-displacement or load-unload curves produced by instrumented indentation system was based on work by Oliver and Pharr [20] and Doener and Nix [30]. Their method assumes that the contact area remains constant while the indenter is

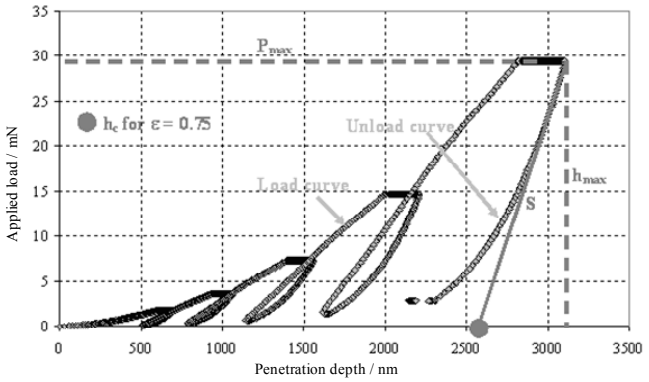

Figure 1. Schematic illustration of indentation load-displacement data when the applied load was 30 mN.

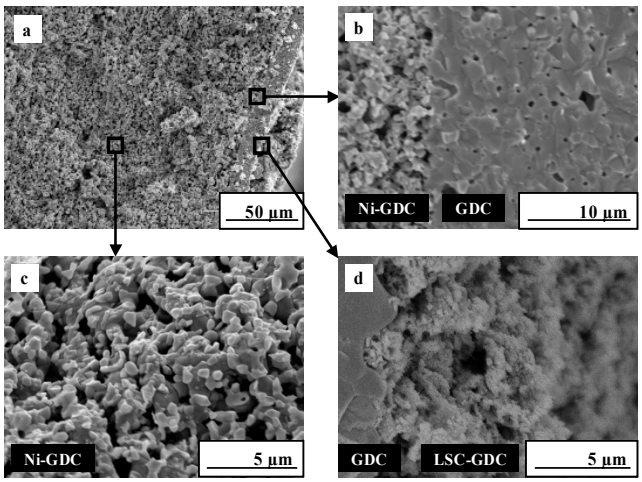

Figure 2. Cross-section SEM micrographs of: (a) anode-supported cell B, (b) anode/electrolyte, (c) anode substrate and (d) electrolyte/cathode.

withdrew and the resulting unloading curve is linear. The hardness was determined from the relationship between the load and the area according to Eq. (1):

$$H = P_{\max} / A_c = P_{\max} / \left(24.5 \cdot h_c^2\right) = P_{\max} / \left[24.5 \cdot \left(h_{\max} - 0.75 \cdot P_{\max} / S\right)\right] \quad (1)$$

where P_{max} is the maximum applied load; A_c, the projected contact area obtained at maximum applied load; h_c, the contact penetration depth and S is the elastic constant stiffness calculated from the load/unload curve for each experiment. On the other hand, the effective or reduced Young's modulus, E_{eff} or E_r, was calculated from the slope of the unloading segment of the load–displacement curve. The effective elastic modulus combines the modulus of the indenter and the specimen according to Eq. (2):

$$1/E_{eff} = \left(1 - \nu^2\right)/E + \left(1 - \nu_i^2\right)/E_i \quad (2)$$

where ν is Poisson's ratio for the test material and E is Young's

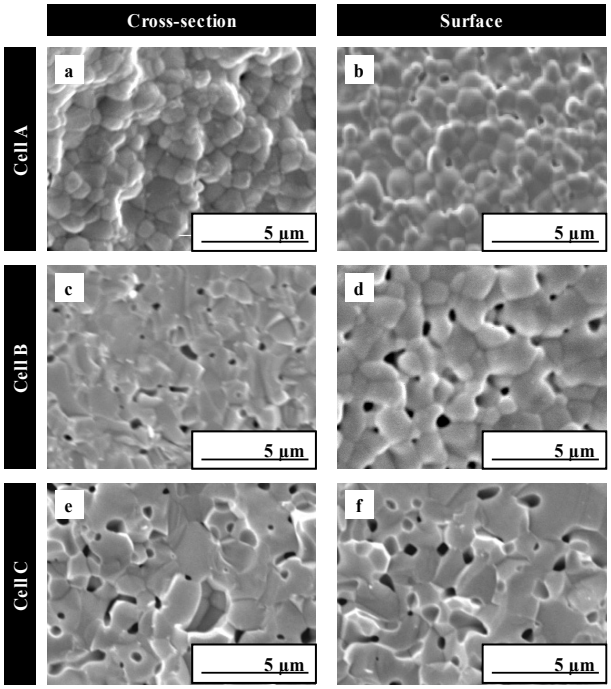

Figure 3. Cross-section and surface SEM micrographs of electrolyte films sintered at different temperatures.

modulus. The subindex i denotes the values of the indenter. For diamond indenter, the elastic constants E_i=1141 GPa and ν_i = 0.07 are often used [20]. While it may seem counterintuitive that one must know Poisson's ratio of the studied material in order to calculate its Young's modulus using the Eq. (2), even a rough estimate, says 0.25 ± 0.1, produces only about a 5% uncertainty in the calculated value of E for many materials. Finally, the values obtained by Oliver and Pharr method were corroborated by optical microscope (M.O) and field emission Hitachi-4100 scanning electron microscope (FE-SEM).

3. RESULTS AND DISCUSSION

3.1. Microstructure of The Cells

Microstructures of the fuel cells were investigated by means of Leica scanning electron microscope (SEM). Fig. 2 shows the cross-section in detail of the single cell B with NiO-GDC anode, GDC electrolyte and LSC-GDC cathode. The electrolyte layer is quite dense and its thickness is about 20 µm (Fig. 2a). The anode-electrolyte and electrolyte-cathode interfaces present a good interfacial adhesion (Fig. 2b,d). The morphology of the anode substrate shown in Fig. 2c is relatively uniform suggesting that pores are homogeneously distributes throughout the substrate. The microstructure of the cathode layer (Fig. 2d) is coarser than that of the anode substrate, in which reduction of NiO to Ni has beneficial effects to create high porosity. The cross-section and surface of electrolyte layers of A, B and C cells are showed in Fig. 3a-f. As can be seen, the electrolyte layer of the cell A (Fig. 3a-b) has many less pores than that of cells B and C (Fig. 3c-f). Although some closed pores are clearly visible in the cell A, no open pore is observed. However, the samples sintered at 1400 and 1450 ºC showed

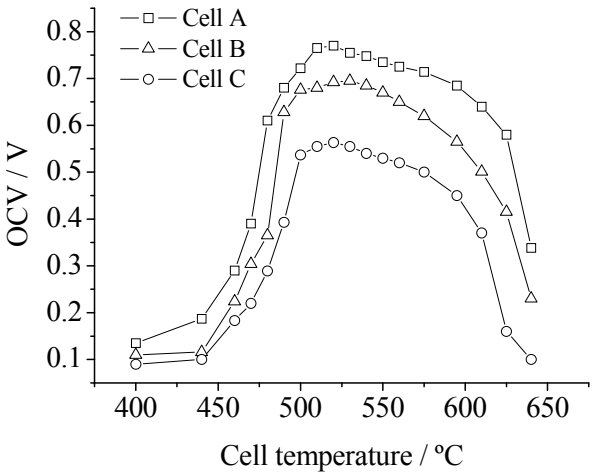

Figure 4. Open circuit voltage (OCV) as a function of furnace temperature for the cells A, B and C.

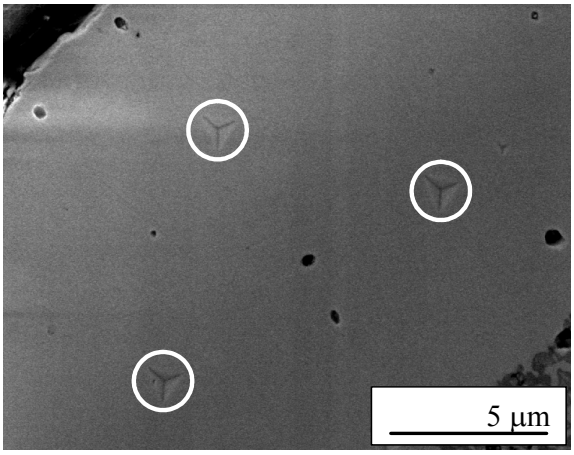

Figure 6. FE-SEM micrographs of residual nanoindentation imprints performed on the electrolyte film of the cell A at 30 mN of applied load.

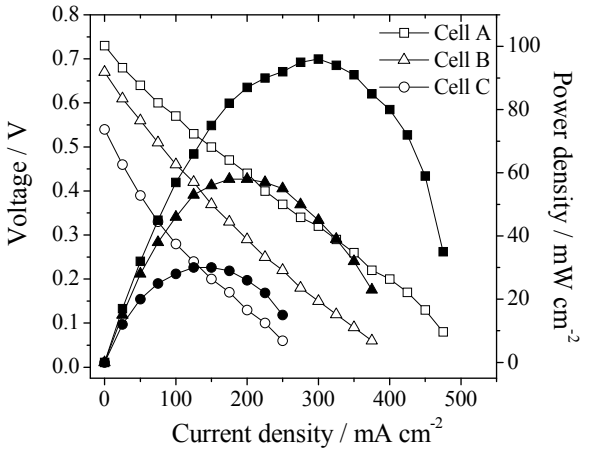

Figure 5. Performance of cells A, B and C in single-chamber SOFC configuration operated at 500 ºC (Tcell ~ 579 ºC). The flows rates were 40 ml/min of propane and 440 ml/min of syntethic air.

open pores, which are formed during sintering treatment. Porosity of the electrolyte film is increased with sintering temperature, which can be due probably to the elimination of oxygen gas produced as consequence of some reduction of Ce^{4+} to Ce^{3+} and/or the rapid volatilization of Co_2O_3 sintering additive [12]. Fig. 3 also reveals the grain microstructure as a function of sintering temperature. The average grain size, estimated from these images, increases from ~0.8 µm to ~3 µm when the sintering temperature increases from 1350 to 1450 ºC.

3.2. Cells Performance

In the SC-SOFCs investigated, the anode has a higher electrocatalytic activity for the partial oxidation of the propane than the cathode. However, the cathode has a higher electrocatalytic activity for the reduction of oxygen. These reactions lead to a low oxygen at the anode locally, while the oxygen partial pressure at the cathode remains relatively high. So, the differences in electrocatalytic properties of the electrodes were sufficiently large to generate important open circuit voltages (OCVs) in the range from 475 to 625 ºC (Fig. 4). The open circuit voltages of the cells A and B were remarkably higher than that of the cell C. The differences in OCVs between cells A and B were not so significant, which indicates there were only some open pores across the GDC thin film of the cell B, according to SEM observation. All of these differences in OCVs must be attributed to the effect of pore density in the electrolyte layer, due probably to the Ni and/or LSC cross-over from anode to cathode and vice-versa, respectively. In general, the OCVs obtained here, even for the cell A with low porosity in the electrolyte, were relatively low. It was attributed to several factors such as non-ideal electrochemical activity of the electrodes and mixed ionic-electronic conductivity (MIEC) of GDC electrolyte because of reduction of some Ce4+ to Ce3+ in the reducing atmosphere of the SC-SOFC [8]. Owing to the reasons mentioned above, similar differences in power densities measured at 579 ºC were observed for the cells studied, which are showed in Fig. 5. The maximum power densities of the cells A, B and C were 97, 58 and 32 mW/cm2, respectively. The results of the voltage/current plot of the cell A performance studied here are similar to those typically observed for operating SC-SOFCs [7,9].

3.3. Mechanical Properties of The Cell Electrolytes

In this study, high load indentation using a sharp tipped indenter was used to measure the hardness and Young's modulus of the electrolytes of the fuel cells A, B and C previously prepared and after OCVs and power densities were measured. Fig. 6 shows micrographs of different nanoindentation imprints obtained by FE-SEM when the applied load was 30 mN. Fig. 7 exhibits several residual nanoindentation imprints performed on the electrolyte for 50 and 100 mN of applied loads. As can be seen in this figure, the size of the residual nanoindentation imprints is lower than the thickness of the electrolyte films. The plastic deformation region produced during the nanoindentation imprints can overestimate the real hardness and Young's modulus value. However, the mechani-

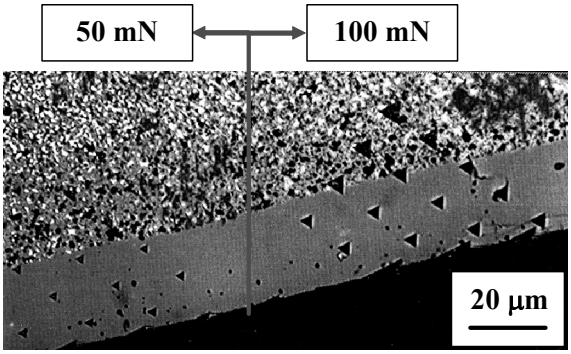

Figure 7. Optical microscope micrographs of nanohardness impressions performed on the electrolyte film of the cell A when the applied load were 50 and 100 mN.

Table 1. Nanohardness and Young's modulus of the electrolyte of the different cells for applied loads of 30, 50 and 100 mN.

Cell	Sintering temperature (ºC)	Applied load (mN)	Hardness, H (GPa)	Young's modulus, E (GPa)
A	1350	30	13.61 ± 0.48	220.6 ± 13.6
		50	12.89 ± 0.94	209.4 ± 10.5
		100	11.60 ± 0.58	186.8 ± 10.2
B	1400	30	11.56 ± 0.36	202.3 ± 12.6
		50	10.48 ± 0.64	195.9 ± 11.6
		100	9.91 ± 0.53	171.4 ± 12.4
C	1450	30	8.13 ± 0.50	178.8 ± 9.85
		50	7.89 ± 0.39	175.1 ± 11.6
		100	7.43 ± 0.24	166.6 ± 12.2

cal properties of the electrolyte can be obtained without contribution of the plastic deformation region when the applied load was lower than 100 mN.

Table 1 lists the calculated hardness and Young's modulus values for each fuel cell when the applied loads were 30, 50 and 100 mN. From these data, the effect of the porosity of the electrolyte film of GDC on the hardness and Young's modulus can be evaluated. Since the mechanical properties of a sintered material depend considerably on its pore density and therefore on its sintering temperature. Higher hardness and Young's modulus values are related to density electrolytes. The values presented for the cell A and B are in agreement with Young's modulus and hardness values reported by Xie et al. and Wang et al. [31,32].

In each of the nanoindentations test series a reduction of hardness when increasing the applied load is observed. This effect is known as indentation size effect (ISE), which is generally attributed to train gradient plasticity that generates geometrically necessary dislocations. For ceramic compounds, where the plasticity is limited, the elastic recovery can be significant. When the ISE is smaller, the density of geometrically necessary dislocations decreases and, as a result, hardness becomes higher at small loads [33].

The analysis of SEM images can be used to determine the profile

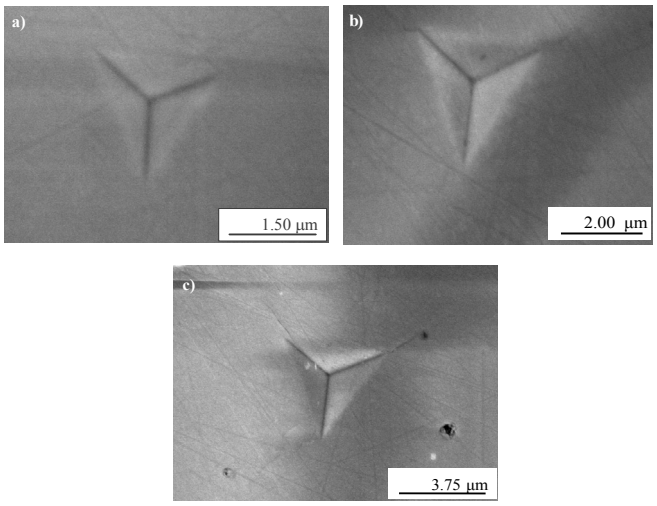

Figure 8. Micrographs of nanoindentation imprints obtained by FE-SEM for the electrolyte film of the cell A when the applied load were a) 30 mN, b) 50 mN, and c) 100 mN.

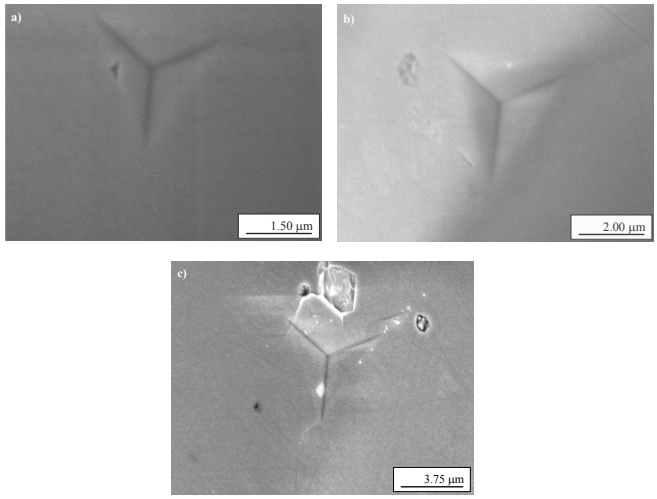

Figure 9. Micrographs of nanoindentation imprints obtained by FE-SEM for the electrolyte film of the cell B when the applied load were a) 30 mN, b) 50 mN, and c) 100 mN.

impressions with nanometer resolution and to provide information about the shape change on unloading. Fig. 8 shows different nanoindentation imprints at different applied loads for electrolyte film of the cell A. As can be seen in this figure, the indentations exhibit a perfect triangular geometry. In this case, the electrolyte presents a high density and a low quantity of pores and defects. All nanoindentation imprints do not present cracks in the corners, radial cracks, porosity behind the imprints and other mechanisms that may produce a reduction of its mechanical properties. Fig. 9 shows a residual nanoindentation imprints for the electrolyte film of the cell B. All residual imprints performed on cell B present porosity besides them. The imprints, reveals a chipping effect (Fig. 9c). Fig. 10 shows a residual imprints for the electrolyte film of the cell C. Fig. 10b exhibits porosity beside its, which produce a reduction of its mechanical properties. The main structural defects, when the

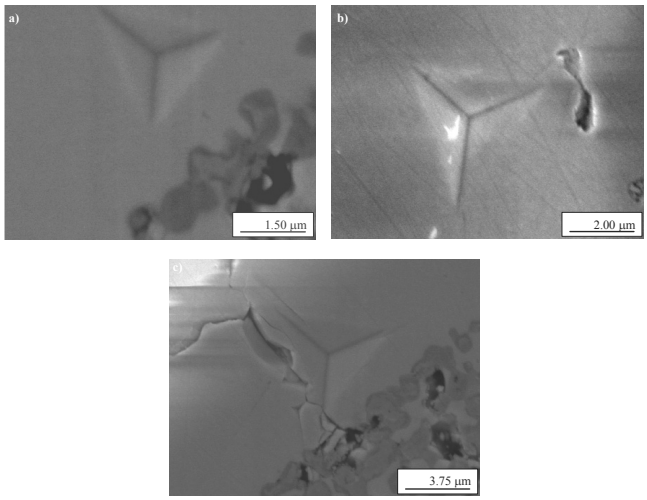

Figure 10. Micrographs of nanoindentation imprints obtained by FE-SEM for the electrolyte film of the cell C when the applied load were a) 30 mN, b) 50 mN, and c) 100 mN.

applied load was 100 mN, are shown in Fig. 10c. The porosity present at the surface of the sample producing a sink-in effect. So, the reduction in the densification of the electrolyte film produces a brittle surface.

4. CONCLUSIONS

The present study has shown that a special attention must be given to the sintering temperature of the thin film GDC electrolyte for SOFCs. Porosity of the electrolyte is increased with sintering temperature in the range from 1350 to 1450 ºC, which can be due to the rapid volatilization of Co_2O_3 sintering additive and/or the elimination of oxygen gas produced as consequence of some reduction of Ce^{4+} to Ce^{3+}. The results indicate that the cell performance and the mechanical properties of a sintered GDC film depend strongly on its sintering temperature. The hardness and Young's modulus of the electrolyte layer decreases with the density of pores. The values presented in this work are in agreement with Young's modulus and hardness values reported by other authors who have used conventional techniques like Vickers indentation. So, the nanoindentation is an ideal technique to determinate the quality and the mechanical properties of the thin film of a SOFC. This work has also revealed that the hardness and Young´s modulus decreased with the increasing of the applied load. This effect is known as indentation size effect (ISE), which is generally attributed to strain gradient plasticity that generated geometrically necessary dislocations.

5. ACKNOWLEDMENTS

The present work was financed by the Spanish MCTE under Project MAT2008-06785-C02-01, XaRMAE (Xarxa de Referència en Materials Avançats per a l'Energia, Generalitat de Catalunya) and the aid of the Commissioner for the University and Investigation of the University Department of Innovation and Company of the Catalan Autonomous Government of Catalonia and the European Social Fund. The authors would like to thank Serveis Cientificotécnics for SEM data and Emilio Jiménez (Centre d'Integritat Estructural i Fiabilitat dels Materials, UPC) for experimental data.

REFERENCES

[1] H. Yahiro, K. Eguchi, H. Arai, Solid State Ionics, 36, 71 (1989).
[2] K. Eguchi, T. Setoguchi, T. Inoue, H. Arai, Solid State Ionics, 52, 165 (1992).
[3] L. Minervini, M. O. Zacate, R. W. Grimes, Solid State Ionics, 116, 339 (1999).
[4] B. C. H. Steele, Solid State Ionics, 129, 95 (2000).
[5] M. Yano, A. Tomita, M. Sano, T. Hibino, Solid State Ionics, 177, 3351 (2007).
[6] T. W. Napporn, X. Jacques-Bédard, F. Morin, M. Meunier, Journal of The Electrochemical Society, 151, 2088 (2004).
[7] Z. P. Shao, C. Kwak, S. M. Haile, Solid State Ionics, 175, 39 (2004).
[8] Z. P. Shao, J. Mederos, William C. Chueh, S. M. Haile, J. Power Sources, 162, 589 (2006).
[9] X. Jacques-Bédard, T. W. Napporn, R. Roberge, M. Meunier, J. Power Sources, 153, 108 (2006).
[10] J. G. Li, T. Ikegami, Y. Wang, T. Mori, J. Am. Ceram. Soc., 86 915 (2003).
[11] T. S. Zhang, J. Ma, Y. J. Leng, S. H. Chan, P. Hing, J. A. Kilner, Solid State Ionics, 168, 187 (2004).
[12] V. Gil, C. Moure, P. Durán, J. Tartaj, Solid State Ionics, 178, 359 (2007).
[13] M. Mogensen, N. M. Sammes, G. A. Tompsett, Solid State Ionics, 129, 63 (2000).
[14] T. S. Zhang, J. Ma, L. B. Kong, P. Hing, Y. J. Leng, S. H. Chan, J. A. Kilner, J. Power Sources, 124, 26 (2003).
[15] W. Lai, S. M. Haile, J. Am. Ceram. Soc., 88, 2979 (2005).
[16] K. Sato, H. Yugami, T. Hashida, J. Mater. Sci., 39, 5765 (2004).
[17] K. R. Reddy, K. Karan, J. Electroceram., 15, 45 (2005).
[18] T. Ishida, F. Iguchi, K. Sato. T. Hashida, H. Yugami, Solid State Ionics, 176, 2417 (2005).
[19] Y. Choi, K. J. Van Vliet, J. Li, S. Suresh, J. Appl. Phys., 94, 6050 (2003).
[20] W. C. Oliver, G. M. Pharr, J. Mater. Res., 6, 1564 (1992).
[21] G. M. Pharr, W. C. Oliver, F. R. Brotzen, J. Mater. Res., 7, 613 (1992).
[22] J. J. Roa, X. G. Capdevila, M. Martínez, F. Espiell, M. Segarra, Nanotechnology, 18, 385701 (2007).
[23] J. J. Roa, E. Jiménez-Piqué, X. G. Capdevila, M. Martínez, M. Segarra, J. Phys: Conf. Ser., 97, 012116 (2008).
[24] M. F. Doerner, D. S. Gardner, W. D. Nix, J. Mater. Res., 1, 845 (1986).
[25] S. Piñol, M. Morales, F. Espiell, J. Power Sources, 169, 2 (2007).
[26] S. Piñol, M. Najib, D. M. Bastidas, A. Calleja, X. G. Capdevila, M. Segarra, F. Espiell, J. C. Ruiz-Morales, D. Marrero-López, P. Nuñez, J. Solid State Electrochem., 8, 650 (2004).

[27]A. I. Fernández, A. Calleja, J. M. Chimenos, M. A. Fernández, X. G. Capdevila, M. Segarra, H. Xuriguera, F. Espiell. J. Sol-Gel Sci. Technol., 36, 11 (2005).
[28]D. Pérez-Coll, D. Marrero-López, P. Núñez, S. Piñol, J. R. Frade, Electrochim. Acta, 51, 6463 (2006).
[29]S. Piñol, J. Fuel Cell Sci. Technol., 3, 434 (2006).
[30]M. F. Doerner, D. S. Gardner and W. D. Nix, J. Mater. Res., 1, 845 (1986).
[31]Y. Xie, X. Zhang, M. Robertson, R. Maric, D. Ghosh, J. Power Sources, 162, 436 (2006).
[32]Y. Wang, K. Duncan, E. D. Wachsman, F. Ebrahimi, Solid State Ionics, 178, 53 (2007).
[33]N. K. Mukhopadhyay, G. C. Weatherly, J. D. Embury, Mater. Sci. Eng. A, 315, 202 (2001).